International Journal of Mechanical, Industrial and Aerospace Sciences
ISSN: 2517-9950
Vol:5, No:11, 2011

Effect of Mesh Size on the Viscous Flow Parameters of an Axisymmetric Nozzle

Rabah Haoui

***Abstract*—**The aim of this work is to analyze a viscous flow in the axisymmetric nozzle taken into account the mesh size both in the free stream and into the boundary layer. The resolution of the Navier-Stokes equations is realized by using the finite volume method to determine the supersonic flow parameters at the exit of converging-diverging nozzle. The numerical technique uses the Flux Vector Splitting method of Van Leer. Here, adequate time stepping parameter, along with CFL coefficient and mesh size level is selected to ensure numerical convergence. The effect of the boundary layer thickness is significant at the exit of the nozzle. The best solution is obtained with using a very fine grid, especially near the wall, where we have a strong variation of velocity, temperature and shear stress. This study enabled us to confirm that the determination of boundary layer thickness can be obtained only if the size of the mesh is lower than a certain value limits given by our calculations.

***Keywords*—**Supersonic flow, viscous flow, finite volume, nozzle

I. Introduction

THIS article presents a calculation of viscous flow in an axisymmetric converging-diverging nozzle. In the present work, we employ a numerical technique to simulate the viscous supersonic flow and the boundary layer thickness in the nozzle especially at the exit section. The gas considered is the air in a standard state composed of 21% of O_2 and 79% of N_2 which is supposed a perfect gas.

The stagnation parameters are 2000K and 500bars, thus the vibration and dissociation of molecules are neglected. These parameters were selected so that the flow at the exit of the nozzle is at 300K, 1bar and with a Mach number equals 5.

The nonlinear partial derivative equations system which governs this flow is solved by an explicit unsteady numerical scheme Goudjo [1] and by the finite volume method haoui [2, 3, and 4]. The flux vector splitting method is used Van Leer [5]. Adequate time stepping parameter and mesh size level are selected to ensure numerical convergence Haoui [6].It is clear that the stationary solution obtained depends on the size mesh used in the numerical Discretization haoui [6].

Rabah Haoui is with Department of Mechanical Engineering University of Science and Technology, Algiers, haoui_rabah@yahoo.fr

We tested convergence for an inviscid flow by using a refining of grid which will enable us to have the exact solution; after this, we refined again the grid near the wall to determine the boundary layer thickness and other parameters.

II. Governing Of Equations

In a Newtonian fluid the viscous stresses are proportional to the rates of deformation. The three-dimensional form of Newton's law of viscosity for compressible flows involves two constants of proportionality, then first dynamic viscosity μ, to relate stresses to linear deformations, and the second viscosity λ, to relate stresses to the volumetric deformation. The viscous stress components are:

$$\tau_{xx} = 2\mu\frac{\partial u}{\partial x} + \lambda\, div(\vec{V}) \quad (1)$$

$$\tau_{yy} = 2\mu\frac{\partial v}{\partial y} + \lambda\, div(\vec{V}) \quad (2)$$

$$\tau_{zz} = 2\mu\frac{\partial w}{\partial z} + \lambda\, div(\vec{V}) \quad (3)$$

$$\tau_{xy} = \tau_{yx} = \mu\left(\frac{\partial u}{\partial y} + \frac{\partial v}{\partial x}\right) \quad (4)$$

$$\tau_{xz} = \tau_{zx} = \mu\left(\frac{\partial u}{\partial z} + \frac{\partial w}{\partial x}\right) \quad (5)$$

$$\tau_{yz} = \tau_{zy} = \mu\left(\frac{\partial v}{\partial z} + \frac{\partial w}{\partial y}\right) \quad (6)$$

Not much is known about the second viscosity λ, because its effect is small in practice. For gases a good working approximation can be obtained by taking the value $\lambda = -\frac{2}{3}\mu$, Schlichting [7].

The Navier-stokes equations in a flux-vector formulation in Cartesian coordinate system is given by

$$\frac{\partial W}{\partial t} + \frac{\partial E}{\partial x} + \frac{\partial F}{\partial y} + \frac{\partial G}{\partial z} = 0 \quad (7)$$

Where the vectors W, E, F and $G$are given by

$$W = \begin{pmatrix} \rho \\ \rho u \\ \rho v \\ \rho w \\ \rho e \end{pmatrix} \quad (8)$$

$$E = \begin{pmatrix} \rho u \\ \rho u^2 + p - \tau_{xx} \\ \rho uv - \tau_{xy} \\ \rho uw - \tau_{xz} \\ (\rho e + p)u - u\tau_{xx} - v\tau_{xy} - w\tau_{xz} + q_x \end{pmatrix} \quad (9)$$

$$F = \begin{pmatrix} \rho v \\ \rho uv - \tau_{xy} \\ \rho v^2 + p - \tau_{yy} \\ \rho vw - \tau_{yz} \\ (\rho e + p)v - u\tau_{xy} - v\tau_{yy} - w\tau_{yz} + q_y \end{pmatrix} \quad (10)$$

$$G = \begin{pmatrix} \rho w \\ \rho uw - \tau_{xz} \\ \rho vw - \tau_{yz} \\ \rho w^2 + p - \tau_{zz} \\ (\rho e + p)w - u\tau_{xz} - v\tau_{yz} - w\tau_{zz} + q_z \end{pmatrix} \quad (11)$$

The heat flux vector q has three components q_x, q_y and q_z given by the Fourier's law of heat conduction relates the heat flux to the local temperature gradient. So:

$$q_x = -k\frac{\partial T}{\partial x},\ q_y = -k\frac{\partial T}{\partial y},\ q_z = -k\frac{\partial T}{\partial z} \quad (12)$$

Where k denotes the coefficient of thermal conductivity, it is function of Prandtl number, viscosity and specific heat.

$$k = Cp.\mu/Pr \quad (13)$$

The energy per unit of mass e is defined as sum of internal energy and kinetic energy such as

$$e = c_v T + \frac{1}{2}(u^2 + v^2 + w^2) \quad (14)$$

III. Axisymmetric Formulation

We do not lose general information by seeking the solution at the points of an infinitely small domain Fig.1. A method developed within the Sinus project of the INRIA Sophia-Antipolis, Goudjo and Désidéri [1], makes it possible to pass from 3D to 2D axisymmetric by using a technique of disturbance of domain. Taking advantage of this finding, here the problem is considered as being axisymmetric.

The system of equations (7) can be written as:

$$mes(c_{i,j})\frac{\partial W_{i,j}}{\partial t} + \sum_{a\in\{x,x',y,y'\}}(F_{i,j}\vec{\imath} + G_{i,j}\vec{\jmath}).\overrightarrow{\eta_a} - H.aire(C_{i,j}) = 0 \quad (15)$$

Where $mes(C_{i,j})$ is the measurement (in m^3) of an infinitely small volume of center (*i,j*). $aire(C_{i,j})$ is the surface of the symmetry plane passing by the center of elementary volume. η_a is the integrated normal. For a detailed calculation of η_a, $aire(C_{i,j})$ and $mes(C_{i,j})$ we refer to work of Goudjo [1]. The third term of the equation expresses the axisymmetric flow condition. Flows, *W*, *F*, *G* and *H* this time are given by:

$$W = \begin{pmatrix} \rho \\ \rho u \\ \rho v \\ \rho e \end{pmatrix} \quad (16)$$

$$F = \begin{pmatrix} \rho u \\ \rho u^2 + p - \tau_{xx} \\ \rho uv - \tau_{xy} \\ (\rho e + p)u - u\tau_{xx} - v\tau_{xy} + q_x \end{pmatrix} \quad (17)$$

$$G = \begin{pmatrix} \rho v \\ \rho uv - \tau_{xy} \\ \rho v^2 + p - \tau_{yy} \\ (\rho e + p)v - u\tau_{xy} - v\tau_{yy} + q_y \end{pmatrix} \quad (18)$$

$$H = \begin{pmatrix} 0 \\ -2\tau_{xy} \\ 2p - 2\tau_{yy} \\ -2u\tau_{xy} - 2v\tau_{yy} + 2v\tau_{zz} + 2q_y \end{pmatrix} \quad (19)$$

Where:

$$\tau_{xx} = 2/3\mu\left(2\frac{\partial u}{\partial x} - \frac{\partial v}{\partial y}\right) \quad (20)$$

$$\tau_{xy} = \tau_{yx} = \mu\left(\frac{\partial u}{\partial y} + \frac{\partial v}{\partial x}\right) \quad (21)$$

$$\tau_{yy} = 2/3\mu\left(2\frac{\partial v}{\partial y} - \frac{\partial u}{\partial x}\right) \quad (22)$$

$$\tau_{xz} = \tau_{zx} = 0 \quad (23)$$

$$\tau_{zz} = 2/3\mu\left(-\frac{\partial u}{\partial x} - \frac{\partial v}{\partial y}\right) \quad (24)$$

$$\tau_{yz} = \tau_{zy} = 0 \quad (25)$$

IV. Discretization In Time

The present numerical method is based on an explicit approach in time and space. The step of time Δt is such as:

$$\Delta t_{i,j} = min\left[\left(\frac{\Delta x.CFL}{\|V\|+a}\right), \left(\frac{(\Delta x)^2.CFL}{2\mu}\right)\right] \quad (26)$$

The *CFL* (Courant, Friedrich, Lewis) is a stability factor Hoffmann [8]. *V* is the velocity of the flow and $a$the speed of sound. Δx is the small length of the mesh at the same point (*i*, *j*). At each time step and for each point (*i*, *j*), the system of equations (27) can be written as:

$$W_{i,j}^{n+1} = W_{i,j}^{n} - \frac{\Delta t_{i,j}}{mes(C_{i,j})}\sum_{a\in\{x,x',y,y'\}}(F_{i,j}{}^{n}\,\vec{\imath} + G_{i,j}{}^{n}\,\vec{\jmath})\,\overrightarrow{\eta_a} + \Delta t_{i,j}\,\frac{aire(C_{i,j})}{mes(C_{i,j})}\,H_{i,j}{}^{n} \quad (27)$$

The choice of the grid plays an important role in determining in the convergence of calculations. Therefore, it is indeed advisable to have sufficiently refine meshes at the places where the gradients of the flow parameters are significantly large.

V. Decomposition Of Van-Leer

In this study, the decomposition of Van-Leer [5] is selected, namely a decomposition of flows in two parts f_{VL}^{-} and f_{VL}^{+} .This decomposition must apply to the present two-dimensional problem by calculating the flow within each interface between two cells. Moreover, through this interface, the normal direction is paramount, thus, a change of reference mark is applied to place in the reference mark of the interface and its normal by the intermediary of a rotation $\boldsymbol{R}$, Fig. 2.

The vector W_E (variable of Euler) is written W_E^R in the new reference mark

$$W_E^R = \begin{pmatrix} \rho \\ \rho \overrightarrow{V_n} \\ \rho\, e \end{pmatrix} \tag{28}$$

where $\overrightarrow{V_n}$ is obtained from $\vec{V}$, via the rotation $\boldsymbol{R}$, in the following way:

$$\vec{V} = \begin{pmatrix} u \\ v \end{pmatrix} \rightarrow \vec{V}_n = \begin{pmatrix} u_n \\ v_n \end{pmatrix} = \begin{pmatrix} cos\,\theta & sin\,\theta \\ -sin\,\theta & cos\,\theta \end{pmatrix} \begin{pmatrix} u \\ v \end{pmatrix} \tag{29}$$

where:

$$cos\,\theta = \frac{\eta_x}{\|\vec{\eta}\|} \ , \quad sin\,\theta = \frac{\eta_y}{\|\vec{\eta}\|} \tag{30}$$

$$\|\vec{\eta}\| = \sqrt{\eta_x^2 + \eta_y^2} \tag{31}$$

The overall transformation $\boldsymbol{R}$ is written overall

$$\boldsymbol{R} = \begin{pmatrix} cos\,\theta & sin\,\theta \\ -\,sin\,\theta & cos\,\theta \end{pmatrix} \tag{32}$$

$$\boldsymbol{R^{-1}} = \begin{pmatrix} cos\,\theta & -sin\,\theta \\ sin\,\theta & cos\,\theta \end{pmatrix} \tag{33}$$

Moreover, at each interface $i + 1/2$, two neighbor states i and $i + 1$ are known. Thus, one can calculate the one-dimensional flow F through the interface, total flow $f(W, \eta)$ being deduced from F by applying the opposite rotation, as:

$$f(W, \vec{\eta}) = \|\vec{\eta}\|.\boldsymbol{R^{-1}}\left(F(W^R)\right) \tag{34}$$

This property makes it possible to use only one component of flow f (F for example) to define the decomposition of flow in two dimensions. Moreover, this method is much easy and simple to implement than the decomposition of flow in two dimensions $f = F\eta_x + G\eta_y$.

The expressions of $F_{VL}^{+}(W^R)$ and $F_{VL}^{-}(W^R)$, where W^R is defined like the transform of W by rotation $\boldsymbol{R}$, are:

$$F_{VL}^{+}(W^R) = \begin{cases} F(W^R) & M_n \geq 1 \\ \begin{pmatrix} \frac{\rho a}{4}\left(\frac{u_n}{a} + 1\right)^2 = f_1^{+} \\ \frac{f_1^{+}}{\gamma}[(\gamma - 1)u_n + 2a] \\ f_1^{+}.v_n \\ \frac{f_1^{+}}{2}\left[\frac{((\gamma-1)u_n + 2a)^2}{\gamma^2 - 1} + v_n^2\right] \end{pmatrix} & |M_n| < 1 \\ 0 & M_n \leq -1 \end{cases} \tag{35}$$

$$F_{VL}^{-}(W^R) = \begin{cases} 0 & M_n \geq 1 \\ \begin{pmatrix} \frac{\rho a}{4}\left(\frac{u_n}{a} - 1\right)^2 = f_1^{-} \\ \frac{f_1^{-}}{\gamma}[(\gamma - 1)u_n - 2a] \\ f_1^{-}.v_n \\ \frac{f_1^{-}}{2}\left[\frac{((\gamma-1)u_n - 2a)^2}{\gamma^2 - 1} + v_n^2\right] \end{pmatrix} & |M_n| < 1 \\ F(W^R) & M_n \leq -1 \end{cases} \tag{36}$$

Where $M_n = u_n/a$, u_n and v_n are the velocity in the reference mark of the interface.

VI. Boundary Conditions

Open (far field) boundary conditions give the most serious problems for the designer of general purpose CFD codes. All CFD problems are defined in terms of initial and boundary conditions. It is important to specify these correctly and understands their role in the numerical algorithm. In transient problems the initial values of all the flow variables need to be specified at all solution points in the flow domain. Since this involves no special measures other than initializing the appropriate data arrays in the CFD code we do not need to discuss this topic further. The present work describes the implementation of the following most common boundary conditions in the discredited equations of the finite volume method: inlet, outlet, wall and symmetry, fig.1.

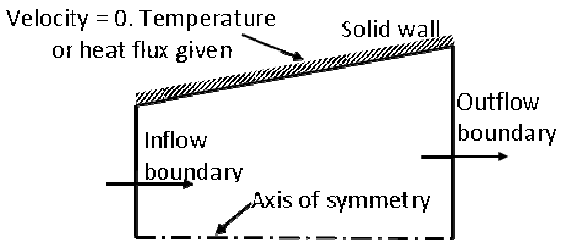

Fig. 1 Boundary conditions

A. Inlet boundary conditions

At the inlet the pressure and temperature are fixed, but the law rate of the flow, M=0.019, obligate us to leave floating one of flow parameters. Here, one chooses to extrapolate the

module of velocity from the interior of the solution domain. This correction allows an adjustment of the flow rate.

B. Body surface

The no-slip condition for the velocity is usually used at the body surface. The temperature gradient at the wall is zero, in accordance with the Fourier equation of heat conduction in the y-direction together with the assumption of zero heat flux at the wall. In this study, we suppose the temperature at the wall is equal the stagnation temperature of free stream. The wall shear stress is calculated by:

$$\tau_w = \mu \left(\frac{\partial V_t}{\partial n}\right)_{wall} \quad (37)$$

Here we assume that the coordinate of the unit vector t is in the direction of the shear force at the wall and the unit vector n is normal at t, Ferziger [9].

C. Axis of symmetry

The conditions at a symmetry boundary are: (i) no flow across the boundary and (ii) no scalar flux across the boundary.

D. Outlet boundary conditions

At the exit of the computational domain the flow is supersonic and the values of the flow parameters are extrapolated from the interior values, including in the boundary layer.

VII. Results And Interpretations

The nozzle tested made up of convergent of conicity $\boldsymbol{\alpha_{conv} = 45°}$ followed by an arc of which the radius $\boldsymbol{r = 2r^*}$ and then divergent of conicity $\boldsymbol{\alpha_{div} = 10°}$ fig. 2. The stagnations pressure and temperature are 100bars and 2000K respectively. The Mach number desired at the exit of the nozzle is 5. The simple laws of a one-dimensional isentropic flow provide us a radius at the exit of the nozzle $\boldsymbol{r_{div} = 0.05\,m}$ for the throat radius $\boldsymbol{r^* = 0.01m}$. The diverging length is thus $\boldsymbol{l_{div} = 0.228m}$. In our calculations we used several sizes of grid while starting with that of figure 2 (116x10), 116 mesh along the axis and 10 mesh along the radius, and then sizes (223x20), (350x30), (466x40), (583x50) and (700x60) with an aim of seeing the effect of refinement on the obtained results.

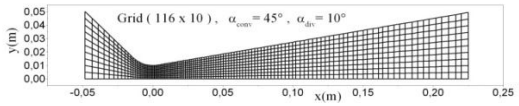

Fig. 2 Grid of solution domain

Firstly, one must to fix the residue value from which the results remain unchanged. For this purpose we use the grid (116x10) since it is the least refined. The parameter which interests us much more in this study is the velocity profile in order to capture the boundary layer thickness fig .3. We observe that the velocity profile is almost the same when the order of the residue is 10^{-5} to 10^{-6}. In the continuation of our work we stop calculations when the residue equal 10^{-5}.

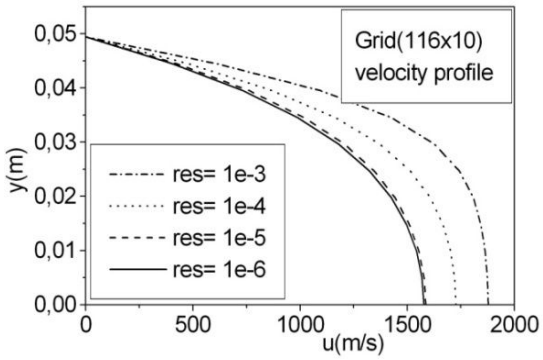

Fig. 3 Velocity profile with various residues

Secondly, one must also fix the size of the grid of the calculation field from which the results remain unchanged, without refinement in the boundary layer. With this intention, one tests six sizes of grid for the same residue fig .4. It is observed that the velocity profile starts to be flattened near the wall, $r = 0.05m$, when the grid is more and more refined. The grid (350x30) is selected since it gives good results and requires less time computing.

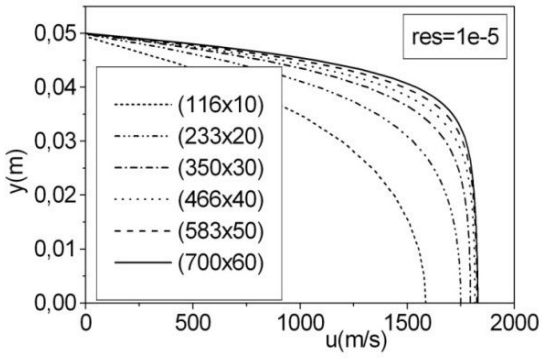

Fig. 4 Velocity profile with various meshes size

Thirdly, one must refine the grid near the wall in order to simulate well the flow parameters in the boundary layer, especially the velocity profile. With this intention, one multiplies the 40% of the meshes near the wall and according to the ray, that is to say 12 meshes, each time by 1, 2, 3, 4 and 5 until where the results remain unchanged fig .5. We notice that the velocity profile becomes even more flattened while approaching the wall; the velocity on the axis is almost always the same. We select the grid (350x78), $ni = 350$ according to x and $nj = 78$ according to y, for the final results. One can even deduce the boundary layer thickness at the exit of the nozzle, when the velocity reaches 95% of the velocity on the axis; the boundary layer thickness is 10.7mm, i.e. 21% of the

radius. If it is admitted that the boundary layer is to 99% of velocity on the axis, its thickness is 18.3mm and it occupies in this case 36% of the radius.

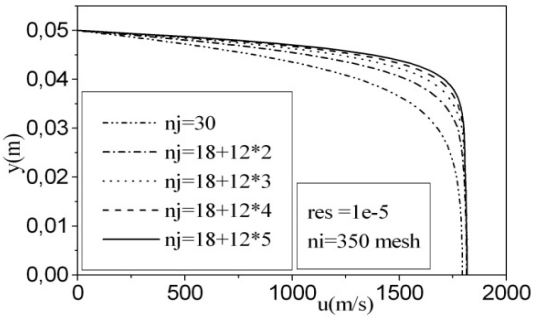

Fig. 5 Velocity profile with various refinements near the wall

Another parameter very significant to calculate in this kind of flow, it is that of the stress τ_{xy}. Figure 6 shows the variation of the shear stress along the radius according to the refinement of the grid in the boundary layer. This profile itself converges to the exact solution for a grid of (350x78). It is observed that the intensity of the stress increases quickly while approaching the wall. The viscous stress at the wall can be calculated from the all stresses at the same point. Figure 7 shows the variation of the stress τ_{wall} along the wall of the nozzle without and with refinement in the boundary layer.

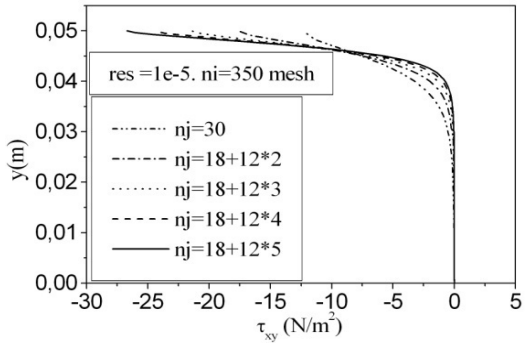

Fig. 6 Profile of shear stress with various refinements near the wall

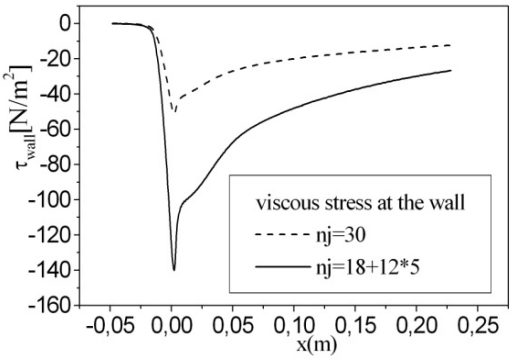

Fig. 7 Viscous stress at the wall with refinement

Concerning the profile of the temperature, the solution also converges to the exact values of the temperature by using the refinement (350x78) fig .8, the wall of the nozzle is adiabatic and the profile of the temperature is thus perpendicular to the wall.

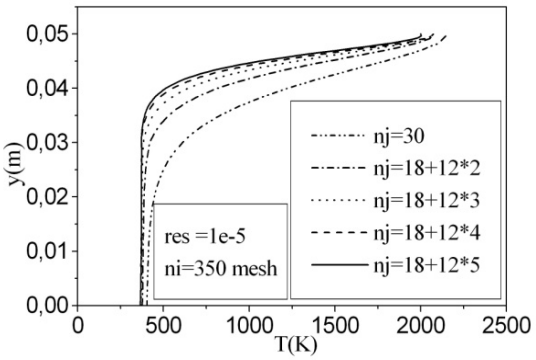

Fig. 8 Temperature profile with various refinements

Finally one represents the flow in the nozzle and one compares it with the inviscid flow. Figure 9 shows the temperature distribution in the nozzle. The thermal boundary layer thickness is visible near the wall.

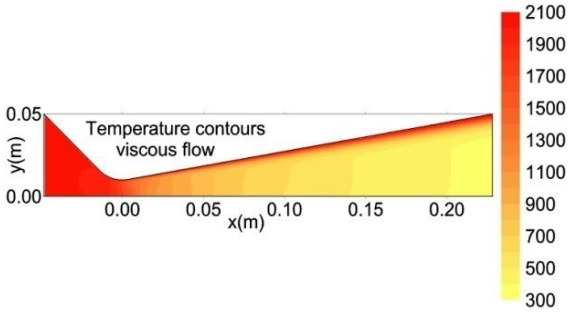

Fig. 9 Temperature contours

A comparison with the inviscid flow is represented on figure 10. The higher part represents the Mach contours of the viscous flow and the lower part represents the Mach contours of the inviscid flow. It is completely clear that the boundary layer influences on the flow parameters in the nozzle, for example at the exit the Mach number is lower than that of the inviscid flow.

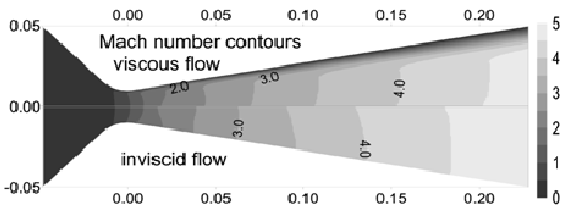

Fig. 10 Number Mach contours comparison

VIII. Conclusion

In conclusion, we can confirm that the results obtained in viscous flow depend strongly on the mesh size in numerical calculation. The program converges, certainly, some is the size of the meshes used, but the exact solution is obtained only if the grid, especially near the wall, is refined much more. The approximation by the infinite volumes method with the non stationary scheme gave good results. Our code is stable, consistent and the solution converges to the exact solution when the grid is very small. The exactitude of our code is carried out by using a mesh size of (350x78) with a residue of 10^{-5}. We saw that the mesh size influences much more the flow parameters in the nozzle, and even on the wall stress. The computer codes which do not take into account of the refinement of the grid, especially near the wall, their results remain at fault compared to the real flow.

References

[1] Goudjo, J.A. Désidéri, " a finite volume scheme to resolution an axisymmetric Euler equations (Un schéma de volumes finis décentré pour la résolution des équations d'Euler en axisymétrique), " Research report INRIA 1005, 1989.

[2] R. Haoui, A. Gahmousse, D. Zeitoun, " Chemical and vibrational nonequilibrium flow in a hypersonic axisymmetric nozzle, " International Journal of Thermal Sciences, article n° 8 , volume 40, (2001), pp787-795.

[3] R. Haoui, "Finite volumes analysis of a supersonic non-equilibrium flow around the axisymmetric blunt body," International Journal of Aeronautical and space Sciences, 11(2), (2010), pp59-68.

[4] R. Haoui," Application of the finite volume method for the supersonic flow around the axisymmetric cone body placed in free stream," WIT press, Fourteenth international conference on computational methods and experimental measurements, pp379-388, Southampton, 2009.

[5] B. Van Leer, "Flux Vector Splitting for the Euler Equations," Lecture Notes in Physics. 170, (1982), 507-512.

[6] R. Haoui, A. Gahmousse, D. Zeitoun, "Condition of convergence applied to an axisymmetric reactive flow," 16th CFM, n°738, Nice, France, 2003.

[7] H. Schlichting, "Boundary-layer theory," 7th edition, McGraw-Hill, New York, 1979.

[8] K. A. Hoffmann, "Computational fluid dynamics for engineers," Volume II. Chapter 14, Engineering Education system, Wichita, USA, pp.202-235, 1995.

[9] J.H. Ferziger & all, "Computational Methods for Fluid Dynamics," Chapter 8, Springer-Verlag, Berlin Heidelberg, New York, pp.217-259, 2002.